Title

Cation-Dependent Light-Induced Halide Demixing in Hybrid Organic—Inorganic Perovskites

Journal

Nano Letters, 18(6)

ISSN

1530-6984

Authors

Sutter-Fella, Carolin M

Ngo, Quynh P

Cefarin, Nicola

et al.

Publication Date

2018-06-13

DOI

10.1021/acs.nanolett.8b00541

Peer reviewed

Cation-Dependent Light-Induced Halide Demixing in Hybrid Organic-Inorganic Perovskites

Carolin M. Sutter-Fella[†#], Quynh P. Ngo[‖#], Nicola Cefarin[&^], Kira L. Gardner[§], Nobumichi Tamura[‡], Camelia V. Stan[‡], Walter S. Drisdell[†], Ali Javey[‖#], Francesca M. Toma[†] and Ian D. Sharp[†+*]*

[†] Chemical Sciences Division, Lawrence Berkeley National Laboratory, Berkeley, CA 94720, US

[‖] Electrical Engineering and Computer Sciences, University of California, Berkeley, California 94720, US

[#] Materials Sciences Division, Lawrence Berkeley National Laboratory, Berkeley, California 94720, US

[&] Joint Center for Artificial Photosynthesis, Lawrence Berkeley National Laboratory, Berkeley, California 94720, US

[^] Department of Physics, Graduate School of Nanotechnology, University of Trieste, 34127 Trieste, Italy

[§] Cyclotron Road, Lawrence Berkeley National Laboratory, Berkeley, California 94720, US

[‡] Advanced Light Source, Lawrence Berkeley National Laboratory, Berkeley, CA 94720, US

[+] Walter Schottky Institut and Physik Department, Technische Universität München, 85748 Garching, Germany

Corresponding Author

*E-mail:
Carolin M. Sutter-Fella: csutterfella@lbl.gov
Ian D. Sharp: sharp@wsi.tum.de (previously Lawrence Berkeley National Laboratory)

Abstract

Mixed cation metal halide perovskites with increased power conversion efficiency, negligible hysteresis, and improved long term stability under illumination, moisture, and thermal stressing have emerged as promising compounds for photovoltaic and optoelectronic applications. Here, we shed light on photo-induced halide demixing using *in-situ* photoluminescence spectroscopy and synchrotron X-ray diffraction (XRD) to directly compare the evolution of composition and phase changes in $CH(NH_2)_2CsPb$-halide (FACsPb-) and CH_3NH_3Pb-halide (MAPb-) perovskites upon illumination, thereby providing insights into why FACsPb-halides are less prone to halide demixing than MAPb-perovskites. We find that halide demixing occurs in both materials. However, the formed I-rich domains accumulate strain for the case of FACsPb-perovskites but readily relax for the case of MAPb-perovskites. The accumulated strain energy is expected to act as a stabilizing force against halide demixing and may explain the higher Br composition threshold for demixing to occur in FACsPb-halides. In addition, we find that while halide demixing leads to a quenching of the high energy photoluminescence emission from MA-

perovskites, the emission is enhanced for the case of FaCs-perovskites. This behavior points to a reduction of non-radiative recombination centers in FACs-perovskites arising from the demixing process. FACsPb-halide perovskites exhibit excellent intrinsic material properties, with photoluminescence quantum yields that are comparable to MA-perovskites. Since improved stability is achieved without sacrificing electronic properties, these compositions are better candidates for photovoltaic applications, especially as wide bandgap absorbers in tandem cells.

ToC

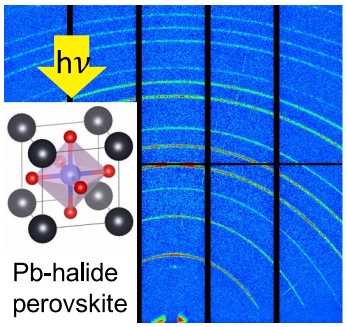

Hybrid metal halide perovskites have recently garnered intense research interest for solar energy conversion and optoelectronic applications due to their excellent properties, such as defect tolerance[1], long minority carrier lifetimes[2,3], and high photoluminescence quantum yields[2,4]. Their general crystal structure is described by ABX_3, typically comprising a monovalent organic cation A (e.g. $CH_3NH_3^+$ [MA], $CH(NH_2)_2^+$ [FA], or inorganic Cs^+), a divalent metal cation B (Pb^{2+}, Sn^{2+}), and a monovalent anion X (I^-, Br^-, Cl^-). Of particular interest is the wide tunability of the optical bandgap of these materials with halide composition, which makes them attractive wide bandgap semiconductors for use as top cells in tandem photovoltaics. For example, alloying of $MAPbI_3$ with Br (i.e. $MAPb(I_{1-x}Br_x)_3$) widens the bandgap from ~1.6 eV (pure I) to ~2.3 eV (pure Br). However, photo-induced reversible halide demixing, in which phase segregation into I-rich and Br-rich domains occurs under illumination, has been reported for $MAPb(I_{1-x}Br_x)_3$ with $0.2 < x < 1$.[5] Such phase separation leads to a local reduction of the bandgap and trapping of charge carriers in the I-rich regions. The result is a significant loss of performance in wide bandgap photovoltaic devices due to reduced open-circuit voltage.

Despite the importance of overcoming halide demixing for achieving stable perovskite-based photovoltaic devices, there remains uncertainty about the underlying mechanism(s) and most studies have focused on MA-perovskites. Currently, strain- or carrier-induced lattice distortion,[6] compositional inhomogeneity,[7] defect-mediated halide migration,[6,8,9] and crystal domain size[10] are actively considered as contributing to halide segregation. In particular, Bischak *et al.* propose that halide demixing is a consequence of localized strain generated from the interaction of charge carriers with the lattice (polaron formation).[6] In this respect, they find that the combination of

mobile halides, long charge carrier lifetimes, and significant electron-phonon coupling are prerequisites for halide demixing.[6] In a different study, Barker *et al.* suggest that defect-assisted halide ion migration away from the illuminated surface, with a slower hopping rate of iodide and a potential dependence on charge carrier generation gradients, results in formation of I-rich regions at the surface.[8] Finally, Rehman *et al.* report that short-range crystalline order facilitates halide demixing, possibly by releasing lattice strain between I-rich and Br-rich domains.[10] In this explanation, they argue that halide segregation in a single crystal would cause significant lattice strain that may not be energetically favorable, while at grain boundaries lattice strain could be more easily accommodated.[10] Importantly, halide demixing is a complex phenomenon and these hypothesized mechanisms are not necessarily mutually exclusive. In addition, vacancy-mediated halide migration is a requirement for demixing processes and, thus, a reduction of defect concentrations and rapid diffusion channels is expected to improve stability under illumination.[6,9]

A potential strategy to circumvent halide demixing is by substitution of the A cation. However, alternative monovalent cations, for example pure FA-[11] and Cs-perovskites[12], are not stable at room temperature and slowly convert to the yellow non-perovskite phase under ambient conditions. Fortunately, the simultaneous incorporation of MA and Br in $FAPbI_3$ perovskites serves to stabilize the perovskite (i.e. alpha) phase,[13] possibly due to a larger dipole interaction of the smaller MA cation with the PbI_6 octahedra[14]. As an indication of the high material quality of mixed cation perovskites, the first reported power conversion efficiency of metal halide perovskite solar cells exceeding 20% was demonstrated with a $MAFAPb(I_{1-x}Br_x)_3$ composition.[15] Calculations suggest that Cs and Rb are more efficient than MA for stabilization of the FA-perovskite phase[16] and first principle computations show that the perovskite phase stabilization

by mixing the A-cations stems from entropic gains.[12] Indeed, $FACsPb(I_{1-x}Br_x)_3$ perovskites have been confirmed by recent reports to exhibit substantially improved stability under illumination[17,18], moisture[17], and thermal stressing[18]. Since there remains uncertainty about the underlying mechanism of halide demixing in high Br-concentration lead halide perovskites, direct comparison of the more stable $FACsPb(I_{1-x}Br_x)_3$ to light-sensitive MA-perovskites provides opportunity to improve understanding of the nature of such instabilities. Elucidation of the mechanism(s) responsible for reversible photo-induced halide demixing is essential for devising strategies for overcoming these processes and developing more stable mixed halide perovskites.

This paper addresses light-induced halide demixing in hybrid high Br-concentration lead halide perovskites as a function of cation composition. We use *in-situ* photoluminescence and synchrotron X-ray diffraction measurements to probe the differences of halide demixing in FACs- and MA-perovskites. The benefit of using synchrotron radiation is its several orders of magnitude higher flux and brilliance, which allows for significantly shorter data collection time and *in-situ* experimentation. Our findings provide mechanistic insights into the enhanced stability against halide demixing in high Br-concentration FACs-perovskites. Although light-induced halide demixing is observed to occur in these FACs-perovskites (shown by photoluminescence), synchrotron X-ray diffraction reveals the absence of peak asymmetry or peak splitting. This suggests that FACsPb-perovskites accumulate strain during halide demixing, whereas strain is relaxed in the case of MA-perovskites. Such accumulated strain is expected to increase the free energy for the demixed state and the inability of the system to relax represents a stabilizing force for high Br FACs-compounds. In both FACs- and MA-perovskites, the

dominant photocarrier recombination behavior is similar with respect to the low energy emission but fundamentally different with respect to the high energy emission. In particular, a reduction of point defect concentrations upon illumination of FACs-perovskites could be responsible for enhanced PL emission compared to the quenching that is observed in MA-perovskites. Beyond better stability, FACsPb-halide perovskites exhibit excellent intrinsic material properties, as deterermined by photoluminescence quantum yield measurements. These results indicate that enhanced stability is achieved alongside reduced non-radiative recombination in FACs-perovskites, thus making them particularly promising wide bandgap semiconductors for optoelectronic applications.

Results

$MAPb(I_{1-x}Br_x)_3$ and $FA_{0.83}Cs_{0.17}Pb(I_{1-x}Br_x)_3$ (in the following shortened to FACsPb-halide or FACs-perovskite) perovskite thin films on glass substrates were fabricated with varying I/(I+Br) ratio by solution processing (see Supporting Information for details) and coated with PMMA to avoid direct contact with atmosphere. For the case of FACsPb-halide perovskites, the Cs content of 17% is chosen in accordance with recent work by Rehman et al.[10] Attempts to synthesize films in a wider composition space with respect to Cs/(Cs+FA)-ratio and halide-content (including Cl) resulted either in a non-perovskite phase or less stable behavior under illumination (Supporting Information, Table S1).

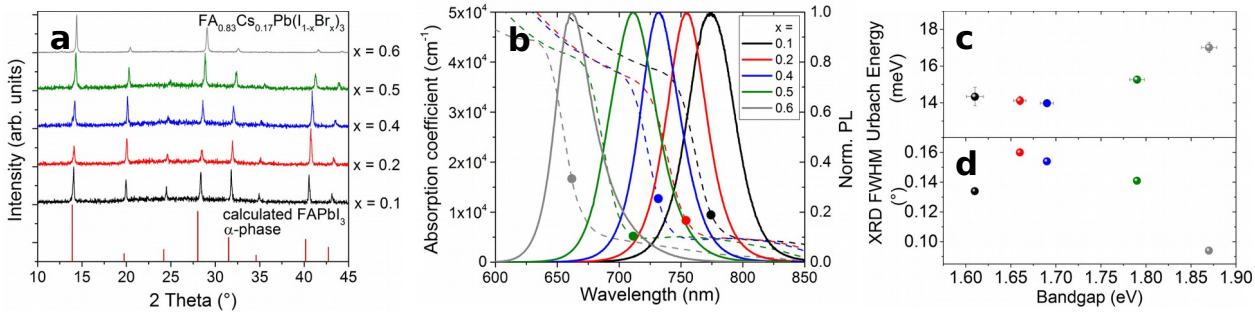

Figure 1. a) X-ray diffraction patterns of the FACsPb($I_{1-x}Br_x$)$_3$ thin films, together with the calculated reference pattern for the alpha (black) $FAPbI_3$ perovskite phase[11]. b) Absorption coefficient (dashed lines) and PL spectra (solid lines) of the samples studied. The filled circles illustrate the position of the PL maximum with respect to the absorption onset. c) Urbach energies extracted from the low-energy PL tail as a function of the bandgap. Error bars in x-axis represent the standard deviation caused by spectral fluctuations (see Supporting Information, Fig. S1) and in y-axis averaging 3 different spots per sample. d) FWHM of the (100) x-ray diffraction peak as a function of the bandgap. The color coding in c) and d) is the same as for panels a) and b).

Structural and optical properties of FACsPb($I_{1-x}Br_x$)$_3$ films with increasing Br content are presented in Figure 1. X-ray diffraction (XRD) measurements confirm crystallization in the alpha (black perovskite) phase[11] (Figure 1a). The samples show high absorption coefficients of >4×10^4 cm^{-1} above the bandgap (Figure 1b, dashed lines) and increasing bandgaps (E_g) from 1.61 eV ≤ E_g ≤ 1.87 eV for 0.1 ≤ x ≤ 0.6. The bandgaps were obtained using Tauc analysis of the absorption coefficients extracted from UV-Vis spectroscopy. The photoluminescence (PL) spectra are overlaid with the corresponding absorption spectra (Figure 1b) and show the PL maximum to be slightly blueshifted with respect to the absorption onsets, with the most pronounced shift of ~20 nm occurring for the sample with the highest Br content in this study (x = 0.6). Such an anti-Stokes shift could be related to the exciton binding energy, self-absorption, or Coulomb interaction.[19] Figure 1c illustrates the Urbach energies extracted from the PL spectra

using the van Roosbroeck–Shockley equation, where the optical emission rate is linked to the absorption coefficient.[20,21] To account for inhomogeneities (see Supporting Information, Fig. S1), Urbach energies were extracted from three independent PL measurements taken across each sample and the standard deviation is included. We also show the Urbach energies of MAPb-halide samples grown by low-pressure vapor-assisted solution process for comparison (Supporting Information, Fig. S2).[22,23] The Urbach energy, which provides a qualitative indication of the crystal lattice distortion caused by defects, dislocations, strain, and impurities, is found to be small, especially considering the fact that these samples are processed at low temperature with simple solution processing, and confirms high crystal quality. For all I/(I+Br)-compositions investigated, the Urbach energy does not exceed 17 meV, which is consistent with the literature value[18] of 16.5 meV for the single composition $FACsPb(I_{0.6}Br_{0.4})_3$. Furthermore, we find that the trend in Urbach energy with increasing x is similar for MAPb- and FACsPb-halide perovskites, but tends to be slightly higher in MAPb-perovskites, particularly at high Br concentration (Supporting Information, Fig. S2). Figure 1d shows the full width at half maximum (FWHM) extracted from the (100)-x-ray diffraction peak of FACsPb-halide perovskites as a function of halide content. Sharp diffraction peaks are observed for all compositions, with highest crystallinity, corresponding to smallest FWHM, observed for the highest Br content ($x = 0.6$). As shown in Figure S3 (Supporting Information), MA-samples are characterized by somewhat smaller XRD FWHM than FACs-samples, indicating larger domain sizes for MAPb-halide perovskites compared to FACs-perovskites.

The intensity of the PL spectra of FACsPb-halides gradually increases (within minutes) upon monochromatic illumination with an Ar-ion laser (514.5 nm excitation wavelength, ~50

mW/cm^2) as depicted in Figure 2. This photo-induced increase is reversible when re-measuring the samples after they were kept in the dark for several minutes. A rise in PL signal (within seconds[6,24]) has been observed previously for low Br-content/pure I MA-perovskites (i.e. phase-stable compositions) and is linked to a filling and stabilization of charge trap states by photo-generated electrons; additionally, the long time constants associated with this process may indicate contributions from the slow motion of ions.[24,25] With higher Br-concentration (x = 0.6), the clear appearance of an additional higher wavelength emission peak is observed (Figure 2c and Supporting Information S4) and is attributed to formation of an I-rich phase with lower bandgap. However, the threshold for photo-induced halide segregation occurs at significantly higher Br content for the case of FACsPb-halide perovskites. In particular, the evolution of a second long wavelength PL emission peak (I-rich phase) in FACs-perovskites appears to only evolve at Br compositions with $x \geq 0.5$ (Figure 2 and Supporting Information Figure S4). This is in agreement with literature, where for the specific composition of x = 0.4, a complete suppression of phase separation has been reported for FACs- but not MAPb-perovskites (note: the power density in that study was as low as 0.03 suns; while we use more than 10 times higher power density here).[18]

A notable difference between the materials studied here is that, for the case of high Br content FACs-perovskites, both the original and the emerging emission peaks (centered around 660-670 nm and 733-740 nm, respectively) increase in intensity with illumination time. In stark contrast, previous studies of $MAPb(I_{1-x}Br_x)_3$ films have shown an almost complete suppression of the short wavelength (i.e. the mixed I-Br phase) emission as the long wavelength I-rich PL emission increases to dominate the spectrum (see Supporting Information Figure S5).[5,26] The single PL

emission in high Br-content MA-perovskites was explained by charge carriers that quickly reach the low bandgap I-rich regions, which act as the main radiative recombination sites.[7,27] In this respect, the difference between MA- and FACs- perovskites is surprising given that for both classes of material, PL emission energy differences between the original mixed I-Br phase and the newly formed I-rich domains is similar, suggesting similar energetic driving forces for charge localization, though the relative band offsets are not yet known. Furthermore, photocarrier diffusion lengths in both MAPb- and FACsPb-halides have been reported to be in the range of a few hundred nm to a few micrometers[10,28], suggesting that, for both cases, they interact with large volumes of material, including regions of the newly formed I-rich phase. To gain more insights in the two phases that form under illumination the Urbach energies of the original phase are compared to the formed phase(s) under illumination (Supporting Information Figure S6). There appears to be a small drop in Urbach energy upon illumination for $x = 0.2$ and 0.5, which implies reduced crystal lattice distortion caused by defects, dislocations, strain, and impurities. However, for higher Br-content, $x = 0.6$, the I-rich domain exhibits a significantly lower E_u compared to the original phase and the Br-rich domain. While these findings are consistent with the improving PL efficiency with time, it remains surprising that PL from the wide bandgap phase is not quenched by charge injection and recombination in the lower bandgap phase, as is observed for the case of MAPb-halide perovksites. Barker *et al.*, explain the much higher PL signal of the I-rich phase compared to the mixed I-Br phase by reduced non-radiative recombination due to the accumulation of carriers in the low-bandgap regions leading to a significant local carrier enhancement. Consequently, the photoluminescence quantum yield from these regions is expected to be very high. This describes the behavior for both the MA- and FACs-perovskites,

where there is significant growth of sub-gap PL emission. However, the PL growth of the high energy peak in the FACs-perovskite cannot be described by this mechanism since funneling of charge carriers to the low bandgap region should: i) overall quench the PL by providing an alternative radiative recombination pathway, and ii) reduce the local carrier concentration such that the degree of state filling is lower and, thus, non-radiative recombination is more probable. From these considerations, it is hypothesized that photo-induced halide demixing in the FACs-perovskite case actually leads to a reduction of recombination centers, not via electronic processes of state filling but rather via the reduction of point defect concentrations. This hypothesis deserves additional studies in the future.

To summarize the *in-situ* PL findings: comparison of MA- versus FACs-perovskites indicates that both material classes exhibit photo-induced halide segregation at sufficiently high Br-concentration, with a threshold composition for halide demixing of approximately $x = 0.2$[5] and $x = 0.5$, respectively. For the case of MA-perovskites, halide segregation results in quenching of emission from the mixed I-Br material and yields a single PL emission dominated by the I-rich phase, while in FACs-perovskites both the I-rich and mixed I-Br PL emission peaks increase in intensity with illumination time. The rates of PL intensity increase with illumination vary with Br content in FACsPb-perovskites and are shown in Supporting Information Figure S7.

Another fundamental difference between MAPb-halides and FACsPb-halides is the changing crystal structure upon halide substitution. $MAPbI_3$ crystallizes in the tetragonal and $MAPbBr_3$ in the cubic structure[29], while both iodide and bromide FA-perovskites adopt the cubic structure.[30,31] Previously, Barker *et al*. noted that for the MA-perovskite case, the composition of the I-rich domains is $x = 0.2$, irrespective of the initial composition,[5] which is similar to the composition at

which the stable phase changes from cubic to tetragonal. Therefore, they hypothesized that the I-enrichment could be limited to compositions of stable cubic phase since transformation to the tetragonal phase could introduce an energetic barrier to additional I-enrichment. However, our results suggest that such an explanation is unlikely, since for the FACs-perovskite case, all compositions are cubic and, nevertheless, the emission wavelength of the low energy peak appears to be constant at ~740-750 nm (Fig. 2 and Supporting Information Fig. S4c), which corresponds to $x \sim 0.3$, assuming any internal strain or quantum size effects in the newly formed phase are negligible. Thus, it appears that iodide enrichment occurs to a limiting composition even in the absence of crystal structure differences.

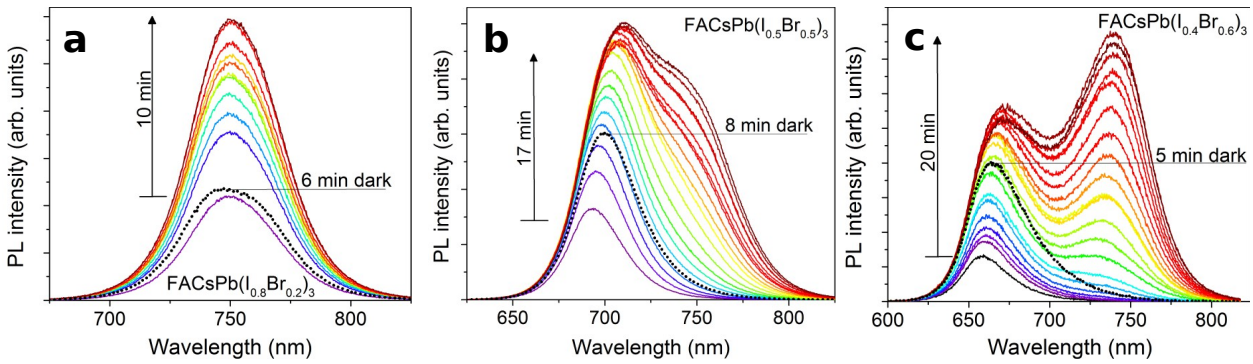

Figure 2. Time evolution of steady-state PL spectra of $FACsPb(I_{0.8}Br_{0.2})_3$ (a), $FACsPb(I_{0.5}Br_{0.5})_3$ (b), and $FACsPb(I_{0.4}Br_{0.6})_3$ (c) thin films taken at ~50 mW/cm^2 illumination density collected in 1 min increments.

In order to provide additional insight into the underlying mechanisms of halide segregation and the effects of these processes on perovskite films, synchrotron X-ray diffraction was performed at the Advanced Light Source, beamline 12.3.2. Unlike conventional lab sources, synchrotron radiation has several orders of magnitude more flux and brilliance, allowing for significantly shorter collection times and *in-situ* characterization of illumination-induced halide demixing. The grazing-angle geometry, in combination with an area detector, enables full XRD patterns to be recorded in the range of $5 < 2\theta < 57°$ within only 60s. Structural analysis of FACs- and MA-halide perovskite thin films (Figure 3) was performed under constant white light illumination with a Xe lamp at ~400 W/m^2 (see Supporting Information Figure S8 for lamp spectrum). In order to enable observation of diffraction peaks from both the original perovskite phase and of potential secondary phases that may evolve during halide demixing, we collected a wide range in 2θ spacing. In the following, we compare a MAPb- to a FACsPb-halide sample, both containing 60% bromide. Figures 3a and 3d show the (100) peaks of the $MAPb(I_{0.4}Br_{0.6})_3$ and $FACsPb(I_{0.4}Br_{0.6})_3$ samples, respectively. Measurements were collected before illumination, during illumination with the Xe lamp, and after ~7 min of relaxation in darkness. Full diffraction patterns can be found in the Supporting Information (Figure S9) and additional diffraction patterns for MA-perovskites with $x = 0.5$, 0.6, and 0.7 are provided in Figure S10.

Constant illumination of the MA-sample leads to a significant peak broadening and evolving peak asymmetry (Figures 3a), while the FACs-sample does not show a change in peak shape but do exhibit a slight broadening (Figures 3d). Diffuse scattering on either side of the (100)-MA-peak leads to a more Lorentzian profile that is typically associated with either strain or defects. The appearance of a new peak towards smaller angles observed in the MA-sample can be related

to a new I-rich phase with different lattice parameters. As mentioned before, the PL emission of the I-rich phase formed under illumination of the FACsPb-sample with $x = 0.6$ would correspond to $x = 0.3$. A change of $\Delta x = 0.3$ translates to a Δ(2 theta) of approximately 0.3° (peak position difference of the original I-Br phase to the I-rich phase with x = 0.3; compare Supporting Information Fig. S3b), which is well within the instrument resolution. This reveals a significant difference between the MA- and the FACs-samples. Namely, there is halide demixing in both samples (seen in PL). However, while the I-rich phases structurally relax in the case of MA, they are not relaxed in the case of the FACs-perovskite. Simultaneously, the (100)-peak integrated intensity (peak area) of the $MAPb(I_{0.4}Br_{0.6})_3$ sample decreases by almost 20% within 30 min of constant illumination (Figure 3b) while the (100)-peak area of the $FACsPb(I_{0.4}Br_{0.6})_3$ sample drops by only ~5% within 60 min of illumination. This may be another indication of either loss of crystallinity or peak splitting caused by some statistically significant portion of the crystallites taking on a tetragonal symmetry upon illumination in the MA samples. Please note the different time intervals of 30 and 60 min for the MA- and FACs-samples, respectively. Aside from broadening of existing peaks and the emergence of peaks indicating small changes of lattice spacing, no entirely new phases (e.g. PbI_2 or non-perovskite) were observed.

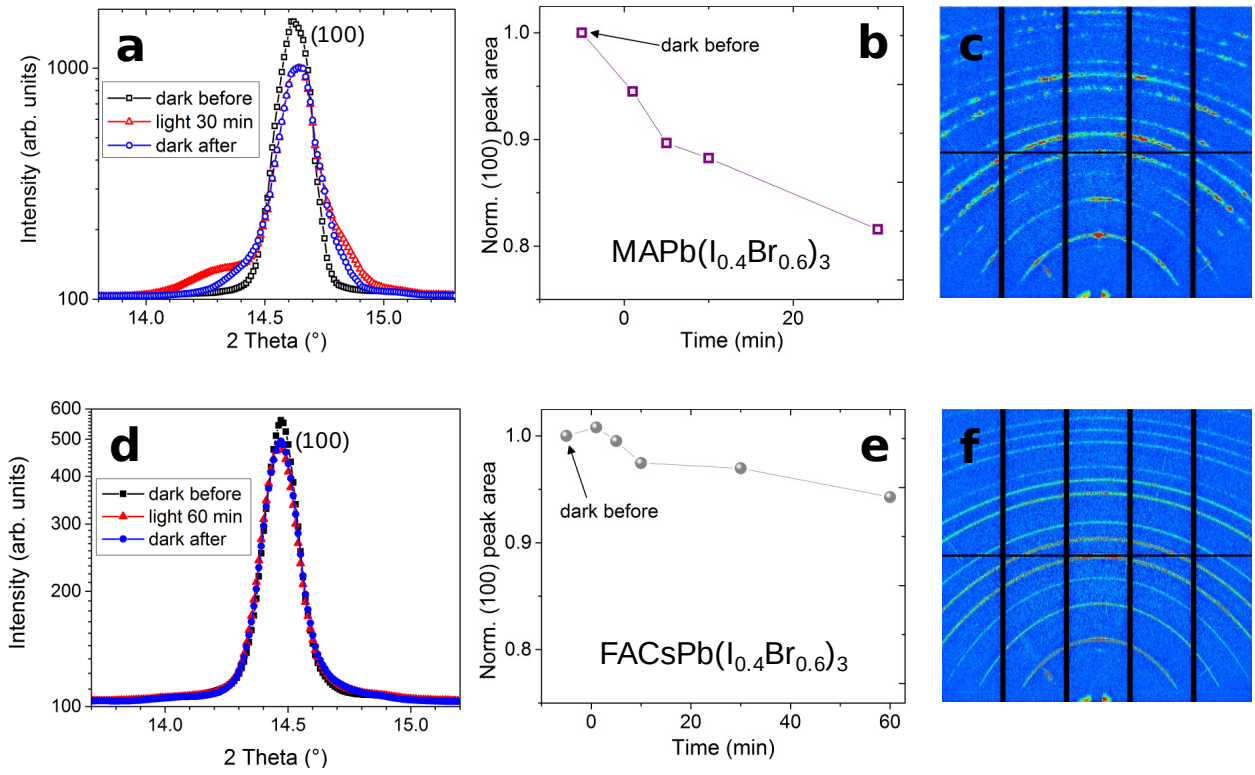

Figure 3. Synchrotron X-ray diffraction data and analysis of the a-c) $MAPb(I_{0.4}Br_{0.6})_3$ and d-f) $FACsPb(I_{0.4}Br_{0.6})_3$ samples. Both samples in cubic symmetry, indexing according to Ref.[29,32]. a+d) (100) diffraction peaks before illumination, during, and after relaxation in the dark. b+e) Normalized peak area under illumination over time. The data points are connected as a guide for the eye. c+f) 2D diffraction patterns after 30 min and 60 min white light illumination, respectively.

The 2D diffraction patterns after white light illumination (Figures 3c+f) illustrate that FACs-perovskites exhibit continuous diffraction rings, reflecting small domain sizes, while the MA-perovskite patterns are spotty, indicating larger domain sizes. The FACs sample has a domain size ≤ 50 nm (using the Scherrer equation) as compared to around 100 nm in the MA-sample. It appears that the halide demixing under illumination shown in the PL measurements (Figure 2) is reflected as a small peak broadening in the X-ray diffraction measurements, but no diffraction peak asymmetry or evidence of peak splitting due to halide demixing as observed for the MA-

sample. For even higher Br-concentration ($x = 0.7$), the FACs-perovskite does not show any peak asymmetry (Supporting Information S11). One suggestion to explain this finding is that I-rich domains nucleate, as evidenced from PL, but remain within individual grains by forming strained grains. The accumulation of stress may act as a stabilizing force against segregation.

PL measurements under continuous illumination (Figure 2) have shown that the dominant recombination processes for MA- and FACs-perovskites are very similar regarding the low energy emission, but not the high energy emission. To shed further light on photocarrier recombination as a function of composition, we study the charge carrier injection dependent recombination behavior by quantitative PL quantum yield measurements (PLQY). Two measurements on different spots were performed for each sample (Supporting Information Figure S12). Figure 4a shows the PLQY curves for $FACsPb(I_{1-x}Br_x)_3$ thin films with $0.1 \leq x \leq 0.6$ versus the injected 1-sun equivalent illumination density. The trend for all Br-compositions is the same: increasing PLQY at low illumination densities up to ~100 suns where the external PLQY reaches a maximum of ~1%, followed by a PLQY drop at illumination densities $\gtrsim$ 1000 suns. At illumination densities ~1-sun, samples with $x = 0.2$ and 0.4 exhibit the highest external PLQY, about 4 times higher than $x = 0.1$. We have previously reported similar results for the MAPb-halide perovskites.[26] A rise in PLQY at low excitation densities, as observed by multiple groups for MAPb-halide perovskites,[4,24,26,33] is characteristic of the filling of trap states until radiative recombination dominates.[24] At 1-sun, the performance of FACsPb-halides is limited by non-radiative trap-assisted recombination, as is the case for MAPb-halides[26,34].

Quantitative PLQY measurements allow for the extraction of the implied open-circuit voltage (V_{oc}) as a measure for the upper limit of the achievable V_{oc} purely based on material quality, circumventing contact formation:[35,36]

$$q V_{oc} \approx kT \ln\left(\frac{J_{sc}}{J_0}\right) + kT \ln PLQY_{ext}$$

$$kT \ln\left(\frac{J_{sc}}{J_0}\right) = V_{oc}^{SQ} \quad ,$$

where V_{oc}^{SQ} is the V_{oc} in the Shockley-Queisser limit in which only interband radiative recombination occurs[37] and is approximated here as E_g - 0.26 eV[38], J_{sc} is the short-circuit current density, and J_0 is the ideal reverse saturation current density for a given material. Figure 4b summarizes the implied V_{oc} calculated for MAPb- and FACsPb- halide perovskites with increasing bandgaps due to Br-alloying, which follow a linearly increasing behavior. The implied V_{oc} for the same bandgap halide perovskite, but MA- versus FACs-cation is similar and slightly superior for FACs-perovskites with $E_g \geq 1.7$ eV. Thus, replacement of MA by FACs leads to enhanced stability without sacrificing the material quality.

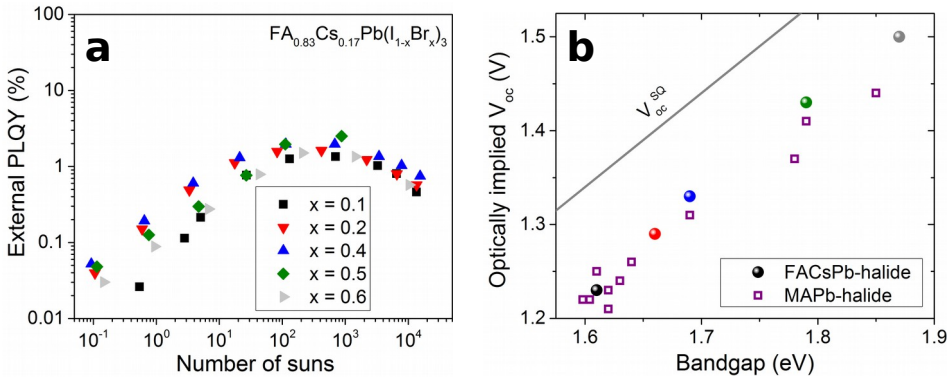

Figure 4. a) PLQY of $FACsPb(I_{1-x}Br_x)_3$ thin films with $0.1 \leq x \leq 0.6$ at increasing illumination densities. b) Implied V_{oc} versus bandgap of FACsPb- and MAPb- halide perovskite samples. The maximum achievable V_{oc}^{SQ} in the radiative limit is drawn as well.

In conclusion, mechanistic insights into the reduced photo-induced halide demixing in high Br-concentration FACsPb-perovskites were provided by combining PL and synchrotron X-ray diffraction measurements. For this study, the evolution of light-induced phase and composition changes in MA- and FACsPb-halide perovskites were directly compared. As a result, we find that FACsPb-halides do show light induced halide demixing, which is not accompanied by a XRD peak broadening nor splitting as typically observed in MA-perovskites. These results suggest that FACs-perovskites are unable to relax strain accumulated during halide demixing, which could serve to partially stabilize the material against phase separation. Although the dominating recombination processes for the low energy emission are similar for MA- and FACs-perovskites, the high energy emission shows the opposite behavior. In particular, the emission is fully quenched in the case of MA-perovskites but increases under illumination for the case of FACs-perovskites. One hypothesis to explain this could be the reduction of the point defect concentration. Beyond better stability, FACs-perovskites exhibit excellent intrinsic material

properties as shown by PLQY measurements comparable to MA-perovskites. Our findings indicate the promise of FACsPb-halide perovskites as stable and efficient top cells for future photovoltaic tandem devices and provide insights into the factors affecting stability of high Br-concentration hybrid lead halide perovskites.

ASSOCIATED CONTENT

Supporting Information.

The Supporting Information is available free of charge on the … Publications website.

AUTHOR INFORMATION

Corresponding Author

*E-mail:

Carolin M. Sutter-Fella: csutterfella@lbl.gov

Ian D. Sharp: sharp@wsi.tum.de (previously Lawrence Berkeley National Laboratory)

Notes

The authors declare no competing financial interest.

Author Contributions

The manuscript was written through contributions of all authors. All authors have given approval to the final version of the manuscript.

Acknowledgements

This manuscript was prepared with support by the Solar Photochemistry Program of the U.S. Department of Energy, Office of Science, Office of Basic Energy Sciences, Division of Chemical, Geological and Biosciences under Contract No. DE-AC02-05CH11231. C. M. S.-F. acknowledges financial support from the Swiss National Science Foundation (fellowships P2EZP2_155586 and P300P2_171420). The photoluminescence measurements were supported by the Electronic Materials program, funded by the Director, Office of Science, Office of Basic Energy Sciences, Materials Sciences and Engineering Division of the U.S. Department of Energy under Contract No. DE-AC02-05CH11231. Synchrotron diffraction measurements were supported in part by the Joint Center for Artificial Photosynthesis, a DOE Energy Innovation Hub, supported through the Office of Science of the U.S. Department of Energy under Award Number DE-SC0004993. This research used beamline 12.3.2 at the Advanced Light Source, which is a DOE Office of Science User Facility under contract no. DE-AC02-05CH11231. K.L.G. was supported by the Cyclotron Road Applied Research Fellowship (DOE-EERE-RPP-AMO-2016) in partnership with Oak Ridge Institute for Science and Education (ORISE).

LITERATURE

(1) Yin, W.-J.; Shi, T.; Yan, Y. Unusual Defect Physics in CH3NH3PbI3 Perovskite Solar Cell Absorber. *Appl. Phys. Lett.* **2014**, *104* (6), 63903.

(2) deQuilettes, D. W.; Koch, S.; Burke, S.; Paranji, R. K.; Shropshire, A. J.; Ziffer, M. E.; Ginger, D. S. Photoluminescence Lifetimes Exceeding 8 Ms and Quantum Yields Exceeding

30% in Hybrid Perovskite Thin Films by Ligand Passivation. *ACS Energy Lett.* **2016**, *1* (2), 438–444.

(3) Moser, J.-E. Perovskite Photovoltaics: Slow Recombination Unveiled. *Nat. Mater.* **2017**, *16* (1), 4–6.

(4) Richter, J. M.; Abdi-Jalebi, M.; Sadhanala, A.; Tabachnyk, M.; Rivett, J. P. H.; Pazos-Outón, L. M.; Gödel, K. C.; Price, M.; Deschler, F.; Friend, R. H. Enhancing Photoluminescence Yields in Lead Halide Perovskites by Photon Recycling and Light out-Coupling. *Nat. Commun.* **2016**, *7*, 13941.

(5) Hoke, E. T.; Slotcavage, D. J.; Dohner, E. R.; Bowring, A. R.; Karunadasa, H. I.; McGehee, M. D. Reversible Photo-Induced Trap Formation in Mixed-Halide Hybrid Perovskites for Photovoltaics. *Chem. Sci.* **2014**, *6* (1), 613–617.

(6) Bischak, C. G.; Hetherington, C. L.; Wu, H.; Aloni, S.; Ogletree, D. F.; Limmer, D. T.; Ginsberg, N. S. Origin of Reversible Photoinduced Phase Separation in Hybrid Perovskites. *Nano Lett.* **2017**, *17* (2), 1028–1033.

(7) Slotcavage, D. J.; Karunadasa, H. I.; McGehee, M. D. Light-Induced Phase Segregation in Halide-Perovskite Absorbers. *ACS Energy Lett.* **2016**, *1* (6), 1199–1205.

(8) Barker, A. J.; Sadhanala, A.; Deschler, F.; Gandini, M.; Senanayak, S. P.; Pearce, P. M.; Mosconi, E.; Pearson, A. J.; Wu, Y.; Srimath Kandada, A. R.; Leijtens, T.; De Angelis, F.; Dutton, S. E.; Petrozza, A.; Friend, R. H. Defect-Assisted Photoinduced Halide Segregation in Mixed-Halide Perovskite Thin Films. *ACS Energy Lett.* **2017**, *2* (6), 1416–1424.

(9) Yoon, S. J.; Kuno, M.; Kamat, P. V. Shift Happens. How Halide Ion Defects Influence Photoinduced Segregation in Mixed Halide Perovskites. *ACS Energy Lett.* **2017**, *2* (7), 1507–1514.

(10) Rehman, W.; P. McMeekin, D.; B. Patel, J.; L. Milot, R.; B. Johnston, M.; J. Snaith, H.; M. Herz, L. Photovoltaic Mixed-Cation Lead Mixed-Halide Perovskites: Links between Crystallinity, Photo-Stability and Electronic Properties. *Energy Environ. Sci.* **2017**, *10* (1), 361–369.

(11) Han, Q.; Bae, S.-H.; Sun, P.; Hsieh, Y.-T.; Yang, Y. (Michael); Rim, Y. S.; Zhao, H.; Chen, Q.; Shi, W.; Li, G.; Yang, Y. Single Crystal Formamidinium Lead Iodide (FAPbI3): Insight into the Structural, Optical, and Electrical Properties. *Adv. Mater.* **2016**, *28* (11), 2253–2258.

(12) Yi, C.; Luo, J.; Meloni, S.; Boziki, A.; Ashari-Astani, N.; Grätzel, C.; M. Zakeeruddin, S.; Röthlisberger, U.; Grätzel, M. Entropic Stabilization of Mixed A-Cation ABX 3 Metal Halide Perovskites for High Performance Perovskite Solar Cells. *Energy Environ. Sci.* **2016**, *9* (2), 656–662.

(13) Jeon, N. J.; Noh, J. H.; Yang, W. S.; Kim, Y. C.; Ryu, S.; Seo, J.; Seok, S. I. Compositional Engineering of Perovskite Materials for High-Performance Solar Cells. *Nature* **2015**, *517* (7535), 476–480.

(14) Binek, A.; Hanusch, F. C.; Docampo, P.; Bein, T. Stabilization of the Trigonal High-

Temperature Phase of Formamidinium Lead Iodide. *J. Phys. Chem. Lett.* **2015**, *6* (7), 1249–1253.

(15) Yang, W. S.; Noh, J. H.; Jeon, N. J.; Kim, Y. C.; Ryu, S.; Seo, J.; Seok, S. I. High-Performance Photovoltaic Perovskite Layers Fabricated through Intramolecular Exchange. *Science* **2015**, *348* (6240), 1234–1237.

(16) Syzgantseva, O. A.; Saliba, M.; Grätzel, M.; Rothlisberger, U. Stabilization of the Perovskite Phase of Formamidinium Lead Triiodide by Methylammonium, Cs, And/Or Rb Doping. *J. Phys. Chem. Lett.* **2017**, *8* (6), 1191–1196.

(17) Lee, J.-W.; Kim, D.-H.; Kim, H.-S.; Seo, S.-W.; Cho, S. M.; Park, N.-G. Formamidinium and Cesium Hybridization for Photo- and Moisture-Stable Perovskite Solar Cell. *Adv. Energy Mater.* **2015**, *5* (20), n/a-n/a.

(18) McMeekin, D. P.; Sadoughi, G.; Rehman, W.; Eperon, G. E.; Saliba, M.; Hörantner, M. T.; Haghighirad, A.; Sakai, N.; Korte, L.; Rech, B.; Johnston, M. B.; Herz, L. M.; Snaith, H. J. A Mixed-Cation Lead Mixed-Halide Perovskite Absorber for Tandem Solar Cells. *Science* **2016**, *351* (6269), 151–155.

(19) Saba, M.; Cadelano, M.; Marongiu, D.; Chen, F.; Sarritzu, V.; Sestu, N.; Figus, C.; Aresti, M.; Piras, R.; Geddo Lehmann, A.; Cannas, C.; Musinu, A.; Quochi, F.; Mura, A.; Bongiovanni, G. Correlated Electron–hole Plasma in Organometal Perovskites. *Nat. Commun.* **2014**, *5*, 5049.

(20) van Roosbroeck, W.; Shockley, W. Photon-Radiative Recombination of Electrons and Holes in Germanium. *Phys. Rev.* **1954**, *94* (6), 1558–1560.

(21) Urbach, F. The Long-Wavelength Edge of Photographic Sensitivity and of the Electronic Absorption of Solids. *Phys. Rev.* **1953**, *92* (5), 1324–1324.

(22) Li, Y.; Cooper, J. K.; Buonsanti, R.; Giannini, C.; Liu, Y.; Toma, F. M.; Sharp, I. D. Fabrication of Planar Heterojunction Perovskite Solar Cells by Controlled Low-Pressure Vapor Annealing. *J. Phys. Chem. Lett.* **2015**, *6* (3), 493–499.

(23) Sutter-Fella, C. M.; Miller, D. W.; Ngo, Q. P.; Roe, E. T.; Toma, F. M.; Sharp, I. D.; Lonergan, M. C.; Javey, A. Band Tailing and Deep Defect States in CH3NH3Pb(I1–xBrx)3 Perovskites As Revealed by Sub-Bandgap Photocurrent. *ACS Energy Lett.* **2017**, *2* (3), 709–715.

(24) Stranks, S. D.; Burlakov, V. M.; Leijtens, T.; Ball, J. M.; Goriely, A.; Snaith, H. J. Recombination Kinetics in Organic-Inorganic Perovskites: Excitons, Free Charge, and Subgap States. *Phys. Rev. Appl.* **2014**, *2* (3), 34007.

(25) deQuilettes, D. W.; Zhang, W.; Burlakov, V. M.; Graham, D. J.; Leijtens, T.; Osherov, A.; Bulović, V.; Snaith, H. J.; Ginger, D. S.; Stranks, S. D. Photo-Induced Halide Redistribution in Organic–inorganic Perovskite Films. *Nat. Commun.* **2016**, *7*, 11683.

(26) Sutter-Fella, C. M.; Li, Y.; Amani, M.; Ager, J. W.; Toma, F. M.; Yablonovitch, E.; Sharp, I. D.; Javey, A. High Photoluminescence Quantum Yield in Band Gap Tunable Bromide Containing Mixed Halide Perovskites. *Nano Lett.* **2016**, *16* (1), 800–806.

(27) Draguta, S.; Sharia, O.; Yoon, S. J.; Brennan, M. C.; Morozov, Y. V.; Manser, J. M.;

Kamat, P. V.; Schneider, W. F.; Kuno, M. Rationalizing the Light-Induced Phase Separation of Mixed Halide Organic–inorganic Perovskites. *Nat. Commun.* **2017**, *8* (1), 200.

(28) Adhyaksa, G. W. P.; Veldhuizen, L. W.; Kuang, Y.; Brittman, S.; Schropp, R. E. I.; Garnett, E. C. Carrier Diffusion Lengths in Hybrid Perovskites: Processing, Composition, Aging, and Surface Passivation Effects. *Chem. Mater.* **2016**, *28* (15), 5259–5263.

(29) Noh, J. H.; Im, S. H.; Heo, J. H.; Mandal, T. N.; Seok, S. I. Chemical Management for Colorful, Efficient, and Stable Inorganic–Organic Hybrid Nanostructured Solar Cells. *Nano Lett.* **2013**, *13* (4), 1764–1769.

(30) Weller, M. T.; Weber, O. J.; Frost, J. M.; Walsh, A. Cubic Perovskite Structure of Black Formamidinium Lead Iodide, α-[HC(NH2)2]PbI3, at 298 K. *J. Phys. Chem. Lett.* **2015**, *6* (16), 3209–3212.

(31) Hanusch, F. C.; Wiesenmayer, E.; Mankel, E.; Binek, A.; Angloher, P.; Fraunhofer, C.; Giesbrecht, N.; Feckl, J. M.; Jaegermann, W.; Johrendt, D.; Bein, T.; Docampo, P. Efficient Planar Heterojunction Perovskite Solar Cells Based on Formamidinium Lead Bromide. *J. Phys. Chem. Lett.* **2014**, *5* (16), 2791–2795.

(32) Baikie, T.; Fang, Y.; Kadro, J. M.; Schreyer, M.; Wei, F.; Mhaisalkar, S. G.; Graetzel, M.; White, T. J. Synthesis and Crystal Chemistry of the Hybrid Perovskite (CH3NH3)PbI3 for Solid-State Sensitised Solar Cell Applications. *J. Mater. Chem. A* **2013**, *1* (18), 5628–5641.

(33) Deschler, F.; Price, M.; Pathak, S.; Klintberg, L. E.; Jarausch, D.-D.; Higler, R.; Hüttner, S.; Leijtens, T.; Stranks, S. D.; Snaith, H. J.; Atatüre, M.; Phillips, R. T.; Friend, R. H. High Photoluminescence Efficiency and Optically Pumped Lasing in Solution-Processed Mixed Halide Perovskite Semiconductors. *J. Phys. Chem. Lett.* **2014**, *5* (8), 1421–1426.

(34) Motti, S. G.; Gandini, M.; Barker, A. J.; Ball, J. M.; Srimath Kandada, A. R.; Petrozza, A. Photoinduced Emissive Trap States in Lead Halide Perovskite Semiconductors. *ACS Energy Lett.* **2016**, *1* (4), 726–730.

(35) Ross, R. T. Some Thermodynamics of Photochemical Systems. *J. Chem. Phys.* **1967**, *46* (12), 4590–4593.

(36) Smestad, G.; Ries, H. Luminescence and Current-Voltage Characteristics of Solar Cells and Optoelectronic Devices. *Sol. Energy Mater. Sol. Cells* **1992**, *25* (1), 51–71.

(37) Shockley, W.; Queisser, H. J. Detailed Balance Limit of Efficiency of P-n Junction Solar Cells. *J. Appl. Phys.* **1961**, *32* (3), 510–519.

(38) Miller, O. D. Photonic Design: From Fundamental Solar Cell Physics to Computational Inverse Design, University of California: Berkeley, 2012.